



Enhanced electrocatalytic properties of Pt–chitosan nanocomposite for direct methanol fuel cell by LaFeO₃ and carbon nanotube



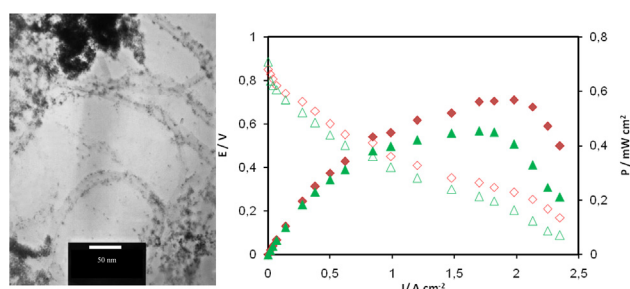
Meissam Noroozifar*, Mozhgan Khorasani-Motlagh, Mehri-Saddat Ekrami-Kakhki, Roghayeh Khaleghian-Moghadam

Department of Chemistry, University of Sistan & Baluchestan, P.O. Box 98155-147, Zahedan, Iran

HIGHLIGHTS

- LaFeO₃NPs are prepared by a rapid microwave-assisted co-precipitation method.
- Catalytic activity of Pt–LaFeO₃ and Pt–LaFeO₃–CNT for methanol oxidation is studied.
- The catalytic activity of PtNPs was enhanced by being mixed with LaFeO₃NPs and CNT.

GRAPHICAL ABSTRACT



ARTICLE INFO

Article history:

Received 25 June 2013
Received in revised form
12 September 2013
Accepted 16 September 2013
Available online 30 September 2013

Keywords:

Platinum
LaFeO₃
Nanoparticles
Carbon nanotube
Methanol oxidation
Fuel cell

ABSTRACT

Incorporation of LaFeO₃ nanoparticles (LaFeO₃NPs) and carbon nanotubes (CNT) into Pt–chitosan for methanol electrooxidation has been studied. LaFeO₃ nanoparticles are successfully prepared by a rapid microwave-assisted co-precipitation method. The formation of LaFeO₃NPs is confirmed by X-ray powder diffraction (XRD), Fourier transformed infrared (FT-IR), scanning electron microscopy (SEM), transmission electron microscopy (TEM) and energy dispersive X-ray (EDX) techniques. Modified glassy carbon (GC) with Pt nanoparticles (PtNPs), LaFeO₃NPs and chitosan (CH) as binder (GC/PtNPs–LaFeO₃NPs–CH) and GC/PtNPs–LaFeO₃NPs–CNT–CH electrodes are prepared by layer by layer technique and their catalytic activity toward methanol oxidation is investigated. It is demonstrated that the catalytic activity of PtNPs can be significantly enhanced by mixing with LaFeO₃NPs and CNT. The Pt–LaFeO₃NPs–CNT catalyst has a better durability compared to the Pt–LaFeO₃NPs catalyst due to the existence of CNT, which prevents dissolution of PtNPs. Moreover, PtNPs–LaFeO₃NPs–CH shows improved methanol oxidation activity, but its direct methanol fuel cells (DMFC) performance is found to be inferior to that measured for PtNPs–LaFeO₃NPs–CNT–CH. The factor influencing PtNPs utilization in the methanol oxidation reaction is intrinsically related to PtNPs formation but using LaFeO₃NPs helps in enhancing the DMFC performance with low Pt loading.

© 2013 Elsevier B.V. All rights reserved.

1. Introduction

Perovskite-type solids specially with general formula, ABO₃ (A = rare earth metals, B = transition metals) have been used as

catalytic materials in technologically important processes [1–3] such as, oxidation of alcohols [4,5], electrochemical evolution/reduction of oxygen, reduction of nitrogen oxides and the chemical oxidation of CO and hydrocarbons [6,7] etc. Recently, various studies on transition metal mixed oxides with the existence of a large amount of oxygen vacancies and excellent electrical conductivities have indicated that the perovskite oxides can be utilized as

* Corresponding author. Tel.: +98 541 241 6464; fax: +98 541 241 6888.
E-mail address: mnoroozifar@chem.usb.ac.ir (M. Noroozifar).

fuel cell electrodes instead of noble metals [8–10]. For example, Mukasyan et al. [11] reported that a variety of ABO_3/Pt compositions with Ru at B-site, exhibit comparable performance with Pt–Ru alloy. It is important that these bifunctional catalysts contain much less platinum than that used in standard ones. These results suggest that such multifunctional catalysts may hold a key for low-cost solution of effective catalyst for DAFCs.

The electrocatalytic activity toward methanol oxidation was affected by both the absorption of methanol as well as the electrical and oxygen ion conductivities of perovskite oxides. The presence of transition metal ions enhances the oxidation of methanol, while simultaneously losing its alcoholic proton to a basic oxide site. Then, the methoxy species might be decomposed with proton abstraction from methoxy moiety and electron transfer to the transition metal and release carbon dioxide. Therefore, the oxidation of the methanol using perovskite electrocatalyst prevents the formation of CO. Also, the residual CO in the fuel flow can be oxidized to CO_2 by the perovskite oxide. These characteristics for the perovskite oxides lead these materials to be functional applications for DMFC electrolyte materials [5].

Polymer electrolyte membrane fuel cell (PEMFC) is an electrochemical device that can use methanol directly or indirectly as a fuel. PEMFC is called the direct methanol fuel cell (DMFC) when methanol is used directly as a fuel. DMFCs are considered as the promising power sources due to simple and easily handling of the fuel, low temperature operation, easy transportation and storage of cheap liquid fuel and high energy density [12,13]. Platinum is known to have the best activity as anode material in the fuel cells, but its surface is easily poisoned by the strongly adsorbed species (CO_{ads}) [14]. CO can be easily removed by incorporating of transition metal especially Ru into the Pt catalyst [15,16], but this improvement requires cost and stability.

Various studies on the preparation of new organic/inorganic hybrid materials and nanocomposites [17] have shown that polymers are a good host material for metal [18–20]. The standard polymer electrolyte membrane, Nafion 117 is widely used as fuel cell membrane. Recently, other membrane materials with lower methanol permeation were investigated as possible replacement for Nafion membrane. Among many polymer electrolyte membranes studied, CH membranes have shown a better performance for applications of low temperature fuel cells [21]. CH is an optically active biopolymer that is characterized by a strong affinity for transition metals. The polymer can be used as a support for the preparation of heterogeneous catalysts in the form of gel beads, colloids, flakes, fibers (including hollow fibers), or immobilized on inorganic supports (silica, alumina, or other metal oxides). The conformation of the polymer (together with its flexibility) is an important advantage for this kind of application [22].

In our previous work, we reported that modified glassy carbon electrode with PtNPs–CH nanocomposite has good performance for the oxidation of methanol. We used dispersion of the platinum nanoparticles in CH matrix to reduce the cost of anode materials. Also, our study showed that addition of elements (Ni, Sn) to PtNPs–CH nanocomposite could enhance the catalyst performance for the oxidation of methanol [23,24]. Here, based on importance of multifunctional catalysts, incorporating effect of perovskite oxide LaFeO_3 and CNT to Pt catalyst for methanol oxidation has been studied. Multifunctional nanocatalysts, PtNPs– LaFeO_3 NPs and PtNPs– LaFeO_3 NPs–CNT dispersed in CH were successfully prepared and their catalytic activity toward methanol oxidation was compared with each other and also with PtNPs–CH and Pt–MNPs–CH ($\text{M} = \text{Ni, Sn}$) nanocatalysts. The effect of some experimental factors such as sulfuric acid and methanol concentration, anodic limit of potential, Pt and LaFeO_3 nanoparticles amounts dispersed in CH and scan rate on the anodic current density and potential of

methanol oxidation were studied and the optimum conditions were suggested.

2. Experimental

2.1. Materials and apparatus

All materials and reagents were purchased from Merck, and used without further purification. Multiwall carbon nanotubes (CNT), with nanotube diameters, OD = 20–30 nm, wall thickness = 1–2 nm, length = 0.5–2 μm and purity > 95% was purchased from Aldrich. CH ([2-amino-2-deoxy-(1-4)- β -D-glucopyranose]), with medium molecular weight, 400,000 Da, was purchased from Fluka and used as received. Acetic acid was diluted to a 1% aqueous solution before use. All solutions were prepared with doubly distilled water. The electrolyte solutions were deoxygenated with nitrogen bubbling before each voltammetric experiment. All glassware were cleaned with freshly prepared aquaregia (3:1; HCl/HNO_3) and rinsed comprehensively with double distilled water prior to use.

FT-IR spectra were obtained by JASCO apparatus 460 plus model with KBr tablet. The XRD spectra were obtained by Philips PC-APD apparatus with graphite monochromatic $\text{CuK}\alpha$ radiation. EDX and SEM images were got by Philips XL30 apparatus. The ultrasonic apparatus with Eurosonic 4D model was used for preparation of the electrode. The centrifuge apparatus with Sigma 101 model was used for separation of the precipitate. Electrochemical investigations were done by SAMA500 Electroanalyser (SAMA Research Center, Iran) controlled by a personal computer. TEM images were taken using a Philips CM120 transmission electron microscope with resolution 2.5 Å.

2.2. Preparation of the nanocatalysts

LaFeO_3 nanoparticles were synthesized by our reported microwave assisted co-precipitation method but here oleic acid was used instead of octanoic acid as surfactant [25] (Scheme 1). The obtained product was characterized by FT-IR, XRD, SEM and EDX techniques. Platinum nanoparticles were prepared by chemical reduction of H_2PtCl_6 with NaBH_4 in the presence of CH. The formation of Pt nanoparticles was confirmed by UV–Vis spectra and TEM observations shown in our previous work [23,24].

2.3. Electrochemical studies

Electrochemical measurements were carried out with an SAMA500 Electroanalyser (SAMA Research Center, Iran) controlled by a personal computer. A standard three-electrode cell was employed. A saturated calomel electrode (SCE) and a platinum electrode were used as the reference and counter electrodes, respectively. The GC electrode with 2 mm of diameter was used as the working electrode substrate. Methanol (1.07 mol L^{-1}) and H_2SO_4 (0.125 mol L^{-1}) served as the electrolyte. All experiments were done at room temperature (25°C) and the scan rate of 100 mV s^{-1} .

2.4. Preparation of the modified electrodes

The GC working electrode with a definite area of 0.0314 cm^2 was polished with $0.05 \mu\text{m}$ alumina slurry to a mirror-finish and prepared as a substrate for catalyst according to our previous works [23,24]. After washing the GC electrode with double-distilled water, it was sonicated in water and absolute ethanol for about 5 min each. Next, the GC electrode was cleaned and activated in freshly prepared deoxygenated $1.0 \text{ mol L}^{-1} \text{ H}_2\text{SO}_4$ by cyclic voltammetry between -1.5 and $+1.5 \text{ V}$ at a scan rate of 100 mV s^{-1} until a stable cyclic voltammetric profile (≈ 15 times) was obtained and then it

was used as the substrate for catalyst. The prepared catalyst (PtNPs–LaFeO₃NPs–CH or PtNPs–LaFeO₃NPs–CNT–CH) suspension was spread by pipette onto the glassy carbon substrate. Evaporation of the solvent formed the deposited catalyst layer.

The PtNPs–LaFeO₃NPs–CH catalyst was prepared as follows. At first, 25 μ l H₂PtCl₆ aqueous solution (1 mol L^{−1}) was mixed with 3 ml CH and stirred in a rotary (rpm 100) for 2 h. Then freshly prepared aqueous solution of NaBH₄ (50 μ l, 2.4 mol L^{−1}) was added to the mixture as reducing agent. To prepare LaFeO₃NPs–CH nanocomposite, 2 mg of LaFeO₃ nano-powders were mixed with 0.5 ml CH and stirred in a rotary (rpm 100) for 2 h. In order to prepare GC/PtNPs–LaFeO₃NPs–CH electrode, 5 μ l of PtNPs–CH solution (8 mmol L^{−1}) and 5 μ l of LaFeO₃NPs–CH suspension were spread by pipette onto the glassy carbon substrate with layer by layer technique. The subsequent evaporation of solvent led to the formation of the deposited catalyst layer.

For preparation of PtNPs–CNT–CH, 25 μ l H₂PtCl₆ aqueous solution (1 mol L^{−1}) was mixed with 1.5 ml CH and stirred in a rotary (rpm 100) for 2 h. 1 mg CNT was separately dispersed in 1.5 ml of CH and sonicated for 30 min to obtain a suspension. Then freshly prepared aqueous solution of NaBH₄ (50 μ l, 2.4 mol L^{−1}) was added to the mixture as reducing agent. Finally, PtNPs–CNT–CH nanocomposite (8 mmol L^{−1}) was prepared. In order to prepared GC/PtNPs–LaFeO₃NPs–CNT–CH electrode, 5 μ l of PtNPs–CNT–CH solution (8 mmol L^{−1}) and 5 μ l of LaFeO₃NPs–CH suspension were spread by pipette onto the glassy carbon surface with layer by layer technique. The subsequent evaporation of solvent led to the formation of the deposited catalyst layer.

2.5. Fuel cell operation

A commercially available catalyzed carbon cloth-diffusion layer (CC-DL) Pt–Ru (30%) (Asian Hydrogen new Science Company (H₂

Engine Company), manufacturing & development Isfahan science and technology town, Isfahan, Iran) was used as the cathode for the fuel cell experiments. The anode catalyst loading was 2.5% Pt–7.5% LaFeO₃–2% CNT onto a commercial CC-DL (2.5PtNPs–7.5LaFeO₃NPs–2CNT/CC-DL). The membrane electrode assembly (MEA) for the low temperature fuel cell was fabricated from Nafion 117 membrane (H₂ Engine Company). The membrane was pre-treated by successive dipping at 80 °C for 30 min each step in 5% (wt) H₂O₂ solution, distilled water, 8 wt% H₂SO₄ solution and then in distilled water again. For preparation of the catalyst-coated membrane, the catalyst ink was sprayed uniformly by an air brush kit (model MBD-116C) onto the pretreated membrane. The active surface area of the single cell was 5 cm². A gas diffusion layer, based on carbon cloth substrates (H₂ Engine Company), was placed on the anode and the cathode sides of the catalyst-coated membrane to form a single cell. The anode and cathode electrodes were hot-pressed onto both sides of a Nafion 117 membrane at 140 °C and 200 psi for 4 min. The MEA was then cooled down to room temperature and assembled in 5 cm² single cells for performance evaluation and stability studies, respectively. The cell operating temperature was set at 80 °C. The flow rates of methanol controlled by a peristaltic pump and humid ml min^{−1} and 100 cm³ min^{−1}, respectively. *I*–*V* curves were obtained galvanostatically with an electronic load, EL200P, Daegil, and controlled by a personal computer.

3. Results and discussion

3.1. Characterization of LaFeO₃NPs

Microwave-assisted synthesis of materials is an active area of research in recent years and various inorganic compounds have been synthesized by this method [26]. It is one of the new methods overcoming the problems occurred in conventional solid-state reaction. The most compelling features of microwave irradiation are dramatically accelerated reaction rates, shorter reaction times and easy workup. Here, LaFeO₃NPs catalyst was synthesized by a rapid microwave-assisted method and the formation of LaFeO₃NPs was confirmed by XRD, FT-IR, EDX and SEM techniques.

X-ray diffraction pattern of LaFeO₃NPs catalyst shown in Fig. 1 confirmed formation of LaFeO₃NPs perovskite single phase. The diffractogram of LaFeO₃NPs catalysts were characteristic of orthorhombic symmetry (PDF 37-1493), space group Pnma (#62) with a main diffraction peak at *d* = 2.776 Å ((1 2 1) plane). In order to determine the lattice parameters of the orthoferrite phase, the following equation [27] was used:

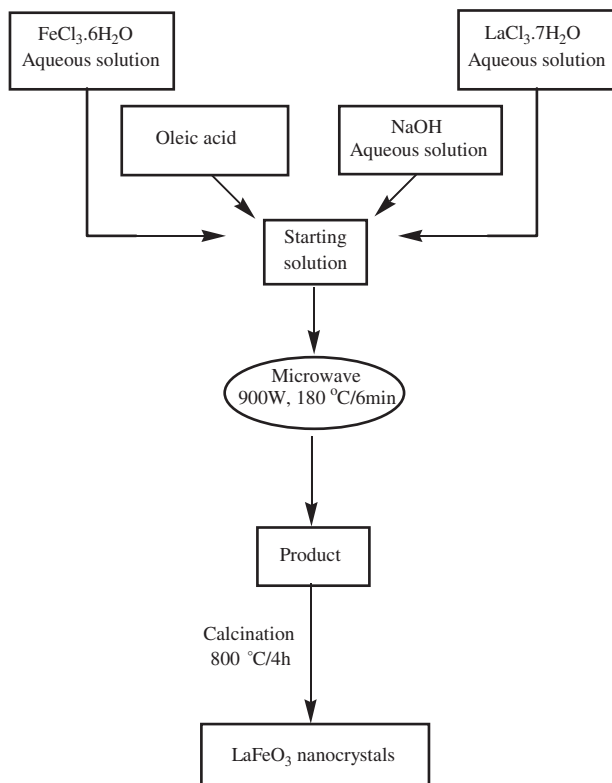
$$\frac{1}{d^2} = \frac{h^2}{a^2} + \frac{k^2}{b^2} + \frac{l^2}{c^2} \quad (1)$$

where *d* is the distance between crystalline planes with Miller indices (*h k l*), and *a*, *b*, and *c* are the lattice parameters. Peaks belonging only to one signal and with a significant diffracted intensity were selected, corresponding to crystalline planes indexed as (1 2 1), (2 0 2) and (2 4 0). The lattice parameters of LaFeO₃ nanocrystals were *a* = 5.55, *b* = 7.85 and *c* = 5.53 Å.

The crystallite size (*D_c*) of LaFeO₃ nanocrystal was also calculated using Debye–Scherrer equation [28]:

$$D_c = \frac{K\lambda}{\beta \cos \theta} \quad (2)$$

where *K* is the so-called shape factor, which usually takes a value about 0.9, λ is the wavelength of the X-ray source used in XRD, β is the breadth of the observed diffraction line at its half-intensity



Scheme 1. The preparation of nanoscale perovskite-type, LaFeO₃.

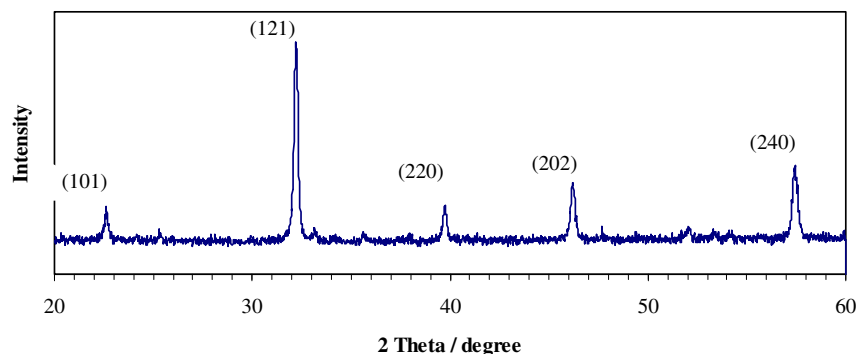


Fig. 1. XRD spectrum of LaFeO₃ nanoparticles.

maximum in radian and θ is the Bragg peak angle. The crystallite size (D_c) of LaFeO₃ nanocrystals was about 35 nm.

The FT-IR spectra of organic surfactant, the product before and after calcination in the frequency range from 4000 to 400 cm^{-1} , are compared in Fig. 2. In FT-IR spectrum of pure organic surfactant, oleic acid, the very broad feature from 2064 to 3006 cm^{-1} is due to O–H stretch of the carboxylic acid. The sharp bands at 2929 and 2857 cm^{-1} are assigned to the asymmetric and symmetric CH₂ stretch, respectively. The intense carbonyl stretch at 1710 cm^{-1} is derived from the C=O of oleic acid carbonyl. In the FT-IR of product before calcination, the characteristic bands of surfactant are shown to be shifted relative to free surfactant. The results for FT-IR measurement indicate that there is an interaction between oleic acid chain and the particles and the surface of the particles was partially covered with the organic ligands. As can see in Fig. 2c, all above bands were disappeared when the product was calcinated. After calcination, the characteristic bands of OH groups disappeared and only strong bands due to the perovskite oxide appeared. In the FT-IR spectrum of the product after calcinations, there are two strong absorption bands at about 552 and 445 cm^{-1} which correspond to Fe–O stretching vibration and O–Fe–O bending vibration of perovskite LaFeO₃, respectively. Their positions are in good agreement with those reported in the literature [29].

The EDX spectrum and SEM image of LaFeO₃ nanocatalyst shown at Fig. 3. The EDX spectrum clearly revealed the presence of La and Fe elements. The element percent obtained from the EDX

spectrum of LaFeO₃ nanocatalyst is shown in the inset of Fig. 3. As seen in SEM image (Fig. 3), LaFeO₃NPs were very homogenate and sphere like with the particle size of about 30–35 nm.

Fig. 4A shows TEM image for LaFeO₃NPs–CH, as seen from this image, LaFeO₃NPs was dispersed very well in CH. Also, TEM image of PtNPs–CNT–CH was shown in Fig. 4B. As seen from Fig. 4B PtNPs with sizes of 2–7 nm are uniformly distributed on CNTs whereas by the modification of PtNPs–CNT–CH with LaFeO₃NPs (Fig. 4C) the nanoparticles no longer coat the CNTs but are distributed in the surrounding solution.

3.2. Electrochemical active surface area (EAS)

The technique of CV was used to determine the Pt electrochemical surface area of the Pt–LaFeO₃NPs and Pt–CNT–LaFeO₃NPs electrodes. Electrochemical active surface area (EAS) can be estimated by cyclic voltammetry (CV) experiments in acid solution (N₂-saturated 0.125 mol L^{−1} H₂SO₄ aqueous solution at room temperature) using the following equation as explained completely in our previous work [23,24].

$$\text{EAS} = \frac{Q_H}{0.21[\text{Pt}]} \quad (3)$$

Where Q_H is the charge for hydrogen desorption, [Pt] represents the platinum loading (mg cm^{-2}) in the electrode, and 0.21 represent the charge required to oxidize a monolayer of H₂ on bright Pt [30].

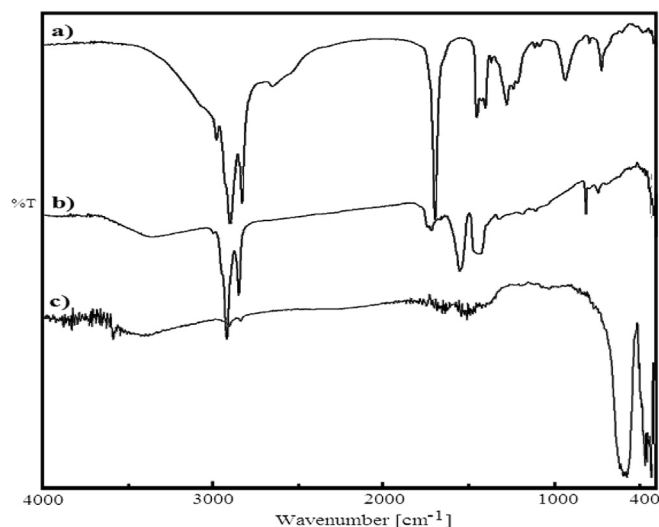


Fig. 2. The FT-IR spectra of the oleic acid (a), the product before calcination (b), the product after calcination (c).

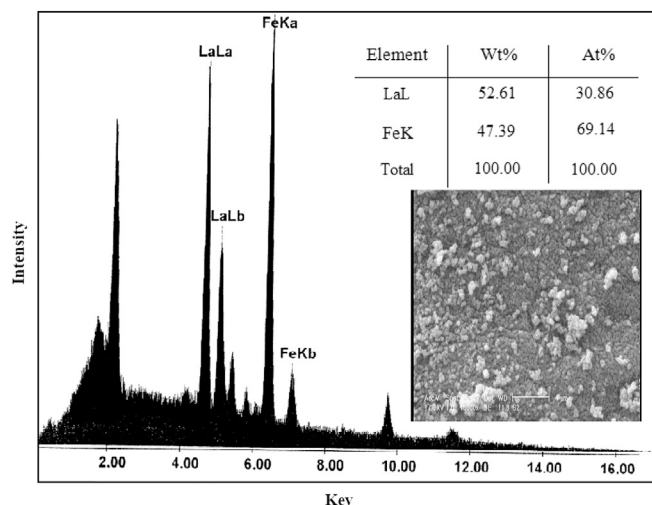


Fig. 3. EDX and elemental composition of LaFeO₃ nanoparticles (inset; SEM image of LaFeO₃ nanoparticles).

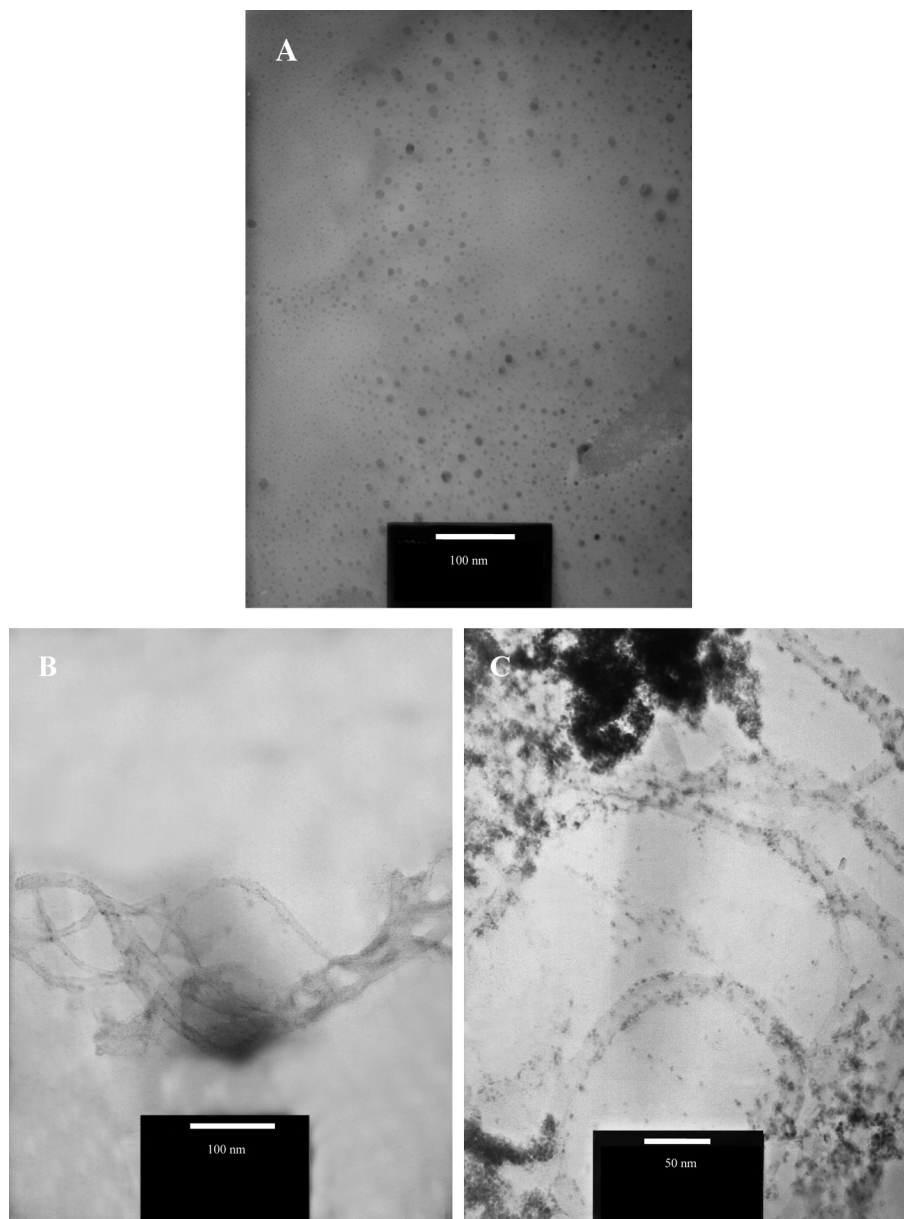


Fig. 4. TEM images of (A) LaFeO₃-CH, (B) PtNPs-CNTs-CH and (C) PtNPs-LaFeO₃-CNTs-CH.

Fig. 5 displayed the CV curves of the as-prepared catalysts in 0.125 M H₂SO₄ solution in the potential range of -0.4 to 1.8 V (vs SCE) for Pt-LaFeO₃NPs and -0.4 to 1.9 V (vs SCE) for Pt-CNT-LaFeO₃NPs nanocatalysts. In Fig. 5, there are two pairs of redox peaks around -0.011 and -0.311 V, which can be ascribed to hydrogen adsorption/desorption on crystal surface sites of Pt. The calculated EAS was $82.2 \text{ m}^2 \text{ g}^{-1}$ Pt for Pt-LaFeO₃NPs-CH and $62.3 \text{ m}^2 \text{ g}^{-1}$ Pt for Pt-CNT-LaFeO₃NPs-CH. ESA for Pt-CNT-LaFeO₃NPs catalyst is lower than that for Pt-LaFeO₃NPs catalyst. This could be due to the CNT structure, which could lead to the blockage of Pt particles inside the pores or encapsulation of Pt particles in the carbon structure.

3.3. Accelerated durability tests

Accelerated durability tests (ADT) of the Pt-LaFeO₃NPs and Pt-CNT-LaFeO₃NPs catalysts are carried out by continuously applying potentials between 0 V and 1.9 V at 50 mV s^{-1} in 0.125 mol L^{-1}

H₂SO₄ solution. In general, the durability of Pt-based electrocatalyst is tested by performing the potential cycling as accelerated durability test in diluted acidic solution [31]. The voltammograms of H₂ adsorption/desorption are used to determine the change of the Pt active surface area for the Pt-LaFeO₃NPs and Pt-CNT-LaFeO₃NPs nanocatalysts by measuring H₂ desorption regions before and after 1000 potential cycles (Fig. 5). It can be seen from Fig. 5 that the EAS value for the Pt-LaFeO₃NPs-CH decreases rapidly from $82.2 \text{ m}^2 \text{ g}^{-1}$ to $63.3 \text{ m}^2 \text{ g}^{-1}$ after the ADT (about 23.0%), indicating a notable decrease of the Pt active surface area due to Pt sintering and the dissolution of Pt metal. While the EAS value for the Pt-CNT-LaFeO₃NPs after the ADT decreases from $62.3 \text{ m}^2 \text{ g}^{-1}$ to $55.4 \text{ m}^2 \text{ g}^{-1}$ with no significant variation (about 11.0%), indicating no considerable decrease of the Pt active surface area. Thus, the degradation rate of the electrode was decreased considerably by adding CNT to the electrode. This clearly indicates that the Pt-CNT-LaFeO₃NPs catalyst is significantly more durable in the acidic solution compared to the Pt-LaFeO₃NPs catalyst. The increase in the anodic

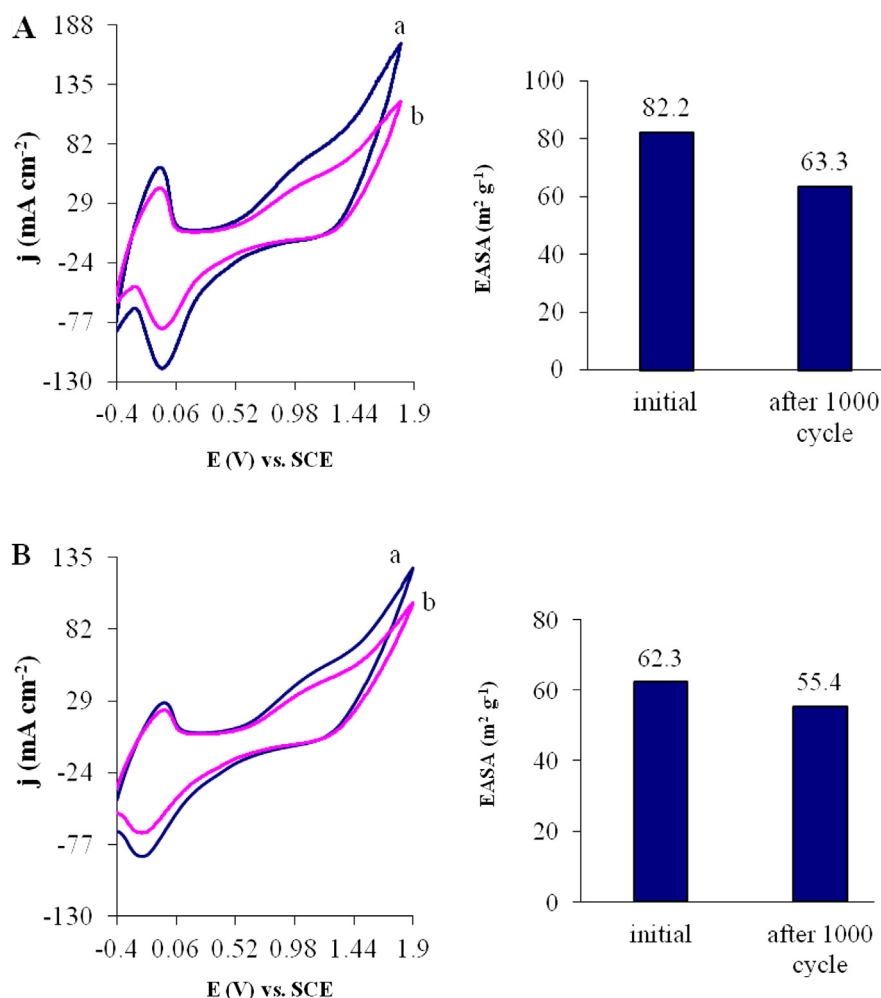


Fig. 5. Cyclic voltammograms of H₂ adsorption/desorption on the A) GC/Pt-LaFeO₃NPs-CH and B) GC/Pt-CNT-LaFeO₃NPs-CH electrodes before (a) and after (b) 1000 potential cycles in 0.125 mol L⁻¹ H₂SO₄ at room temperature with a scan rate of 50 mV s⁻¹.

peak current density of methanol oxidation could be attributed to the significant electronic conductivity of the MWCNTs and their greatly electrochemical accessible surface area.

3.4. Oxidation of methanol on modified glassy carbon with Pt-LaFeO₃NPs-CH and Pt-CNT-LaFeO₃NPs-CH nanocomposites

Electrochemical properties of modified GC electrodes have been investigated by cyclic voltammetry in 1 mol L⁻¹ CH₃OH and 0.125 mol L⁻¹ H₂SO₄ aqueous solution and the typical cyclic voltammograms for GC/CH, GC/Pt-LaFeO₃NPs-CH and GC/Pt-CNT-LaFeO₃NPs-CH are shown in Fig. 6 (CV at GC electrode is not shown, which is similar to that of GC/CH electrode). As seen in Fig. 6a, no current peaks of methanol oxidation can be observed on GC and GC-CH electrodes showing that GC and GC/CH substrates have no obvious electrocatalytic activity for methanol oxidation. The cyclic voltammogram for methanol oxidation obtained on GC/Pt-LaFeO₃NPs-CH electrode is shown in Fig. 6b and high electrocatalytic activity is observed. As seen in Fig. 6b and c, two peaks of methanol oxidation can be observed obviously in the range of 0.0–1.6 V for the electrodes. In Fig. 6b, two oxidation peaks, which are related to the oxidation of methanol (*I_f*) and the corresponding intermediates (*I_b*) produced during the methanol oxidation (*I_f/I_b* = 1.94), can be observed obviously at 1.204 (*E_f*) and 0.449 V (*E_b*), respectively. The onset potential of a current rise for methanol

oxidation on GC/Pt-LaFeO₃NPs-CH electrode was 0.195 V. As observed in Fig. 6c, two oxidation peaks (*I_f/I_b* = 2.13) can be obtained obviously at 1.101 (*E_f*) and 0.487 V (*E_b*) on the GC/Pt-CNT-LaFeO₃NPs-CH electrode. The onset potential for methanol oxidation on GC/Pt-CNT-LaFeO₃NPs-CH electrode was 0.026 V. The characteristics of the CV curves and the corresponding peak potentials (*E_p*) are in agreement with other works [32–34]. As can clearly be seen, the anodic peak potential and the onset potential of methanol oxidation on GC/Pt-CNT-LaFeO₃NPs-CH electrode was more negative than that of GC/Pt-LaFeO₃NPs-CH electrode. Also, the *I_f/I_b* ratio of GC/Pt-CNT-LaFeO₃NPs-CH electrode was more than that of GC/Pt-LaFeO₃NPs-CH electrode showing that Pt-CNT-LaFeO₃NPs-CH nanocomposite had more catalytic activity for methanol oxidation with respect to Pt-LaFeO₃NPs-CH nanocomposite. The catalytic activity of GC/Pt-LaFeO₃NPs-CH and Pt-CNT-LaFeO₃NPs-CH electrodes are compared with the catalysts prepared in our previous works [23,24] and shown in Table 1. As observed in Table 1, GC/Pt-LaFeO₃NPs-CH and Pt-CNT-LaFeO₃NPs-CH electrodes had higher catalytic activity than that of Pt, Pt-Sn, Pt-Ni and Pt-Ni-Sn-CH nanocatalysts according to the anodic current density, onset potential. The catalytic activity of the catalysts was as follows:

Pt-CNT-LaFeO₃NPs-CH > Pt-LaFeO₃NPs-CH > Pt-Ni-SnNPs-CH > Pt-NiNPs-CH > Pt-SnNPs-CH > PtNPs-CH

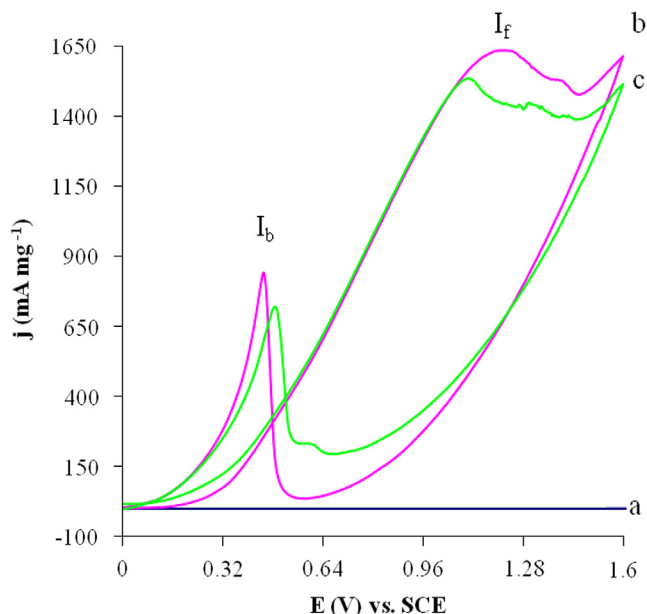


Fig. 6. Cyclic voltammograms for methanol oxidation in 1.0 mol L⁻¹ methanol and 0.125 mol L⁻¹ H₂SO₄ on a) GC/CH, b) GC/Pt–LaFeO₃NPs–CH and c) GC/Pt–CNT–LaFeO₃NPs–CH electrodes (CV on GC electrode is not shown, which is similar to that of GC–CH electrode).

Our results showed that the oxidation current density on GC/Pt–LaFeO₃NPs–CH and GC/Pt–CNT–LaFeO₃–CH is considerably higher than that of obtained at glassy carbon modified electrode by Pt with other elements such as Ru, Co and Mn and is considerably higher than that obtained at glassy carbon modified electrode by Pt–Ni–Pb, Pt–Ru–Ni, Pt–Ru–Co, Pt–Ru–Fe, PtRuSn, Pt–Ru and Pt [35–46].

3.5. Important parameters of methanol oxidation

Our investigations showed that different parameters such as concentration of sulfuric acid as the electrolyte, methanol concentration, Pt and LaFeO₃ nanoparticles' amounts and scan rate were the main factors influencing the performance of the proposed modified electrodes for oxidation of methanol. So, these parameters must be optimized.

3.5.1. Effect of sulfuric acid concentration

The effect of sulfuric acid concentration on the anodic current density (j_f) and potential (E_f) of the methanol oxidation on GC/Pt–LaFeO₃NPs–CH and GC/Pt–CNT–LaFeO₃NPs–CH electrodes are studied and the best result for all electrodes is observed with sulfuric acid 0.125 M, so the experiments were done in this concentration of sulfuric acid.

3.5.2. Effect of methanol concentration

The effect of methanol concentration on the anodic current density of methanol oxidation on the GC/Pt–LaFeO₃NPs–CH and

GC/Pt–CNT–LaFeO₃NPs–CH electrodes is shown in Fig. 7. It is clearly observed that the anodic current density increases with increasing methanol concentration and levels off at concentrations higher than 1.0 mol L⁻¹. This effect may be due to the saturation of active sites on the surface of the electrode. According to this result, the optimum concentration of methanol to obtain a higher current density may be considered as about 1.0 mol L⁻¹.

As seen in the cyclic voltammograms obtained on GC/Pt–LaFeO₃NPs–CH electrode (Fig. 7A), when the methanol concentration increased from 0.08 to 1.0 mol L⁻¹, the E_f and E_b shifted toward positive direction from 0.681 to 1.204 V and 0.095 to 0.449 V, respectively. This may result from the following reason: The increase of the methanol concentration will increase the poisoning rate of the Pt catalyst and cause a shift of the oxidative removal of the strongly adsorbed intermediates to a more positive potential [47]. I_f/I_b decreases from 3.652 to 1.941 when the methanol concentration increases from 0.08 to 1.0 mol L⁻¹. This is due to increasing the poisoning rate of the Pt catalyst with adsorbed intermediates.

As observed in Fig. 7B, cyclic voltammograms were also obtained on GC/Pt–CNT–LaFeO₃NPs–CH electrode in different concentrations of methanol. The same behavior was obtained on GC/Pt–CNT–LaFeO₃NPs–CH electrode. When the methanol concentration increased from 0.08 to 1.0 mol L⁻¹, the E_f and E_b shifted toward positive direction from 0.67 to 1.067 V and 0.071 to 0.454 V, respectively.

3.5.3. Effect of Pt and LaFeO₃ amounts

Chronoamperometry experiments were carried out at potential value 1.2 V in order to investigate the catalytic activities of the GC/Pt–LaFeO₃NPs–CH electrode in different amounts of Pt and LaFeO₃ nanoparticles. Representative chronoamperograms obtained for different electrodes with the constant amount of LaFeO₃ nanoparticles (2 mg) and different concentrations of PtNPs are shown in Fig. 8A. As seen in Fig. 8A, there is an initial current decay in less than 7 s and the best result was obtained for the electrode of Pt 8 mM composition. In the case of electrode containing constant concentration of PtNPs and different amount of LaFeO₃NPs (Fig. 8B), the best result was obtained for the electrode with 2 mg of LaFeO₃NPs and an initial current decay in less than 5 s. In all chronoamperometry experiments, the electrode containing Pt and LaFeO₃ nanoparticles (Pt 8 mmol L⁻¹ and LaFeO₃NPs 2 mg) showed the highest anodic current density value, which corroborate with the results obtained by cyclic voltammetry.

3.5.4. Effect of scan rate

Cyclic voltammograms at different scan rates (ν) in the range between 30 and 150 mV s⁻¹ for oxidation of methanol on GC/Pt–LaFeO₃NPs–CH and GC/Pt–CNT–LaFeO₃NPs–CH electrodes were studied. It is indicated that the peak current densities increases linearly with the scan rate.

The current density and potential of the anodic oxidation peak of methanol oxidation on GC/Pt–LaFeO₃NPs–CH and GC/Pt–CNT–LaFeO₃NPs–CH electrodes are plotted vs the square root of

Table 1

Electrochemical data for methanol oxidation on different electrodes with various catalysts (ref. electrode is SCE, scan rate is 100 mV s⁻¹).

Catalyst composition	Onset methanol oxidation potential (V)	E_f (V)	j_f (mA cm ⁻²)	Electrolyte	Ref.
Pt–CH	0.18	0.92	190.47	1.3 M MeOH + 0.125 M H ₂ SO ₄	[23]
Pt–Ni–CH	0.20	1.17	335.4	1.5 M MeOH + 0.125 M H ₂ SO ₄	[24]
Pt–Sn–CH	0.20	1.16	230.9	1.5 M MeOH + 0.125 M H ₂ SO ₄	[24]
Pt–Ni–Sn–CH	0.16	1.25	416.8	1.5 M MeOH + 0.125 M H ₂ SO ₄	[24]
Pt–LaFeO ₃ –CH	0.195	1.204	406.53	1.0 M MeOH + 0.125 M H ₂ SO ₄	This work
Pt–CNT–LaFeO ₃ –CH	0.026	1.101	381.34	1.0 M MeOH + 0.125 M H ₂ SO ₄	This work

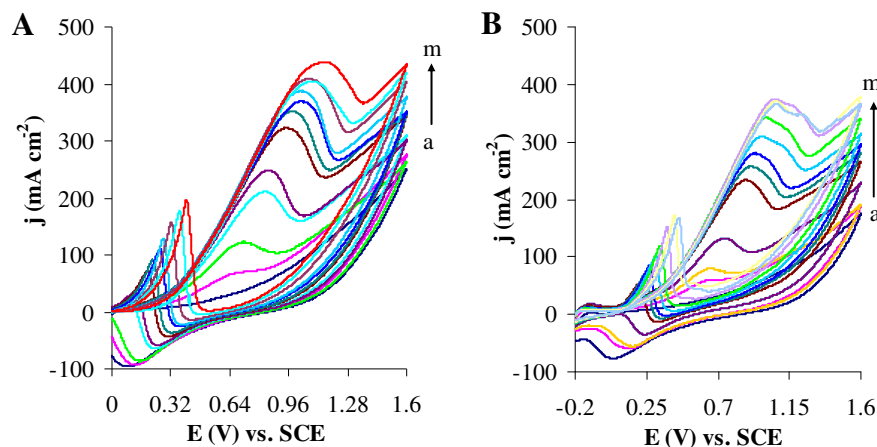


Fig. 7. Cyclic voltammograms for methanol oxidation on A) GC/Pt–LaFeO₃NPs–CH and B) on GC/Pt–CNT–LaFeO₃NPs–CH electrodes in 0.125 mol L^{−1} H₂SO₄ in different concentration of methanol: a) 0.08, b) 0.16, c) 0.24, d) 0.31, e) 0.39, f) 0.47, g) 0.55, h) 0.62, i) 0.70, j) 0.77, k) 0.85, l) 0.92, m) 1.0 M.

the scan rate ($v^{1/2}$) and scan rate (v) in Fig. 9. In Fig. 9A and B, the current densities of the anodic oxidation peak of methanol oxidation on GC/Pt–LaFeO₃NPs–CH electrode are plotted as a function of the square root of the scan rate ($v^{1/2}$) and the scan rate (v), respectively. The current densities of methanol oxidation peak on GC/Pt–CNT–LaFeO₃NPs–CH electrode are plotted as a function of the square root of the scan rate (Fig. 9E) and the scan rate (Fig. 9F). As can be clearly seen, there is a linear correlation between the anodic current density and $v^{1/2}$, suggesting that the kinetics of the overall process is controlled by mass-transport.

Also, the potential of the anodic oxidation peak of methanol oxidation on GC/Pt–LaFeO₃NPs–CH (Fig. 9C) and GC/Pt–CNT–LaFeO₃NPs–CH electrodes (Fig. 9D) are plotted vs the square root of the scan rate ($v^{1/2}$) and scan rate (v). As seen in Fig. 9C and D, the potential of the oxidation peak of methanol oxidation increases with increasing of the scan rate.

3.6. Single cell performances

In order to understand the enhanced performance of the Pt–LaFeO₃ catalyst (5Pt–15LaFeO₃/CC-DL) in the presence of LaFeO₃NPs as an oxygen storage component, single cell tests are carried out for the MEA made with the 5Pt–15LaFeO₃–2CNT/CC-DL catalyst as the anode, and the commercial Pt–Ru/C catalyst as the cathode for CH₃OH/O₂. For the sake of comparison, the I – V

characteristic of the MEA made with the 5Pt–15LaFeO₃/CC-DL as the anode is also prepared. From the I – V characteristics (Fig. 10), the open circuit voltages (OCV) of the single cells using the 5Pt–15LaFeO₃–2CNT/CC-DL and 5Pt–15LaFeO₃/CC-DL as anodes and commercial Pt–Ru/C catalysts as cathode are 0.85 V and 0.88 V, respectively. However, the 5Pt–15LaFeO₃/CC-DL catalyst shows a lower polarization loss than Pt–LaFeO₃NPs/CNT catalyst. For the CH₃OH–O₂ cell, the 5Pt–15LaFeO₃–2CNT/CC-DL catalyst generated 1.98 A cm^{−2} at 0.33 V and a maximum power density of 0.60 W cm^{−2}. In the same condition, the 5Pt–15LaFeO₃/CC-DL catalyst generated 1.70 A cm^{−2} at 0.27 V and a maximum power density of 0.45 W cm^{−2}. The fuel cell results also indicated that deposited Pt particles provided adequate electron pathway and improved the electrical conductivity of the LaFeO₃NPs support.

4. Conclusion

In this work, Pt–LaFeO₃–CH and Pt–CNT–LaFeO₃–CH nanocomposites were successfully synthesized. GC/Pt–LaFeO₃NPs–CH and GC/Pt–CNT–LaFeO₃NPs–CH electrodes were prepared as active electrocatalysts for methanol oxidation. Our results showed that the addition of LaFeO₃ nanoparticles and carbon nanotube into Pt catalyst and use of a more porous matrix of CH can significantly improve the electrode performance for methanol oxidation. The activity of Pt–CNT–LaFeO₃–CH nanocomposite for methanol

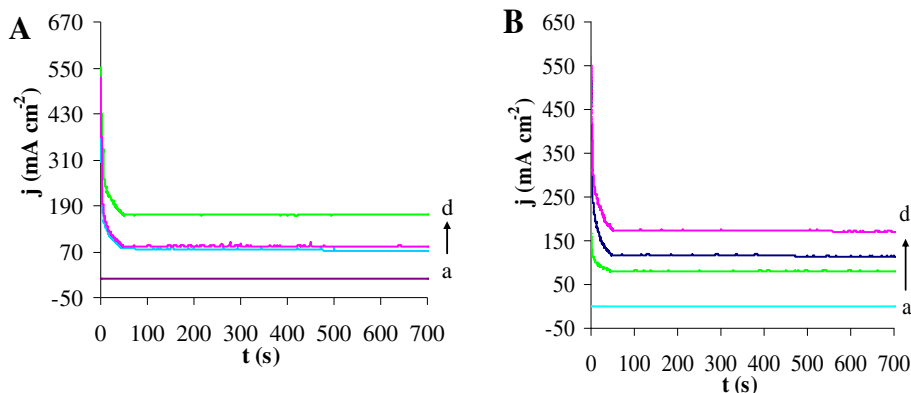


Fig. 8. Chronoamperometry for methanol oxidation in 1.0 M methanol and 0.125 mol L^{−1} H₂SO₄ on GC/Pt–LaFeO₃NPs–CH electrocatalyst with different A) concentrations of Pt: a) 0, b) 4, c) 12, d) 8 mmol L^{−1}, and B) amount of LaFeO₃NPs: a) 0, b) 3, c) 1, d) 2 mg (chronoamperometry on GC electrode is not shown, which is similar to that of GC–CH electrode).

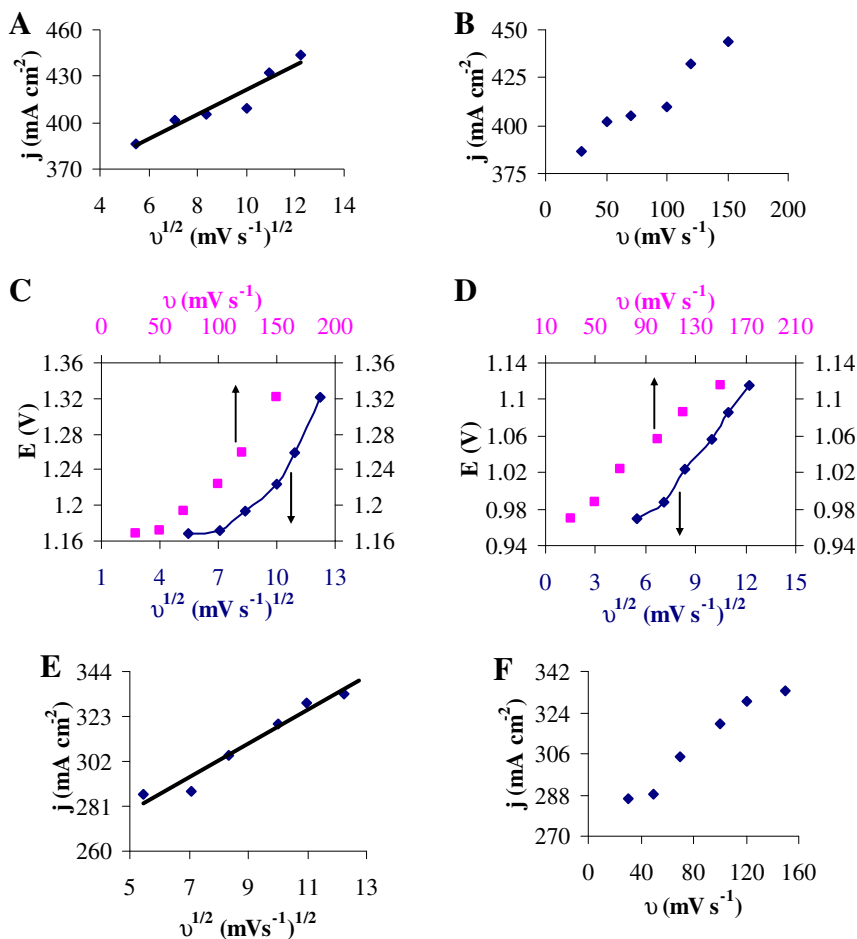


Fig. 9. Plot of anodic current density of methanol oxidation peak at GC/Pt–LaFeO₃NPs–CH electrode vs square root of scan rate (A) and vs scan rate (B), plot of the anodic peak potential of methanol oxidation at GC/Pt–LaFeO₃NPs–CH (C) and GC/Pt–CNT–LaFeO₃NPs–CH electrode (D) vs square root of scan rate and scan rate, variation of the anodic current density of methanol oxidation peak at GC/Pt–CNT–LaFeO₃NPs–CH electrode vs square root of scan rate (E) and vs scan rate (F).

oxidation in acid medium is higher than that of Pt–LaFeO₃–CH catalyst according to the anodic peak potential and onset potential of methanol oxidation. The factor influencing PtNPs utilization in the methanol oxidation reaction is intrinsically related to PtNPs formation but using LaFeO₃NPs helps in enhancing the DMFC performance with low Pt loading.

Acknowledgment

We thank University of Sistan and Baluchestan (USB) for financial support.

References

- [1] L.G. Tejuca, J.L.G. Fierro, J.M. Tascon, in: D.D. Eley, H. Pines, P.B. Wiesz (Eds.), *Advances in Catalysis*, Academic Press, Inc., California, 1989, pp. 237–328.
- [2] E.J.M. O'Sullivan, E.J. Calvo, in: R.G. Compton (Ed.), *Comprehensive Chemical Kinetics*, Elsevier, Amsterdam, 1987, pp. 247–360.
- [3] S. Trasatti, in: J. Lipkowsky, N. Ross Philip (Eds.), *The Electrochemistry of Novel Materials*, VCH Publishers, Inc., New York, 1994, pp. 207–295.
- [4] M.L. Faro, G. Monforte, A. Stassi, M. Minutoli, V. Antonucci, V. Modafferi, P. Antonucci, A.S. Arico, *Adv. Sci. Technol.* 72 (2010) 255–260.
- [5] H.C. Yu, K.Z. Fung, T.C. Guo, W.L. Chang, *Electrochim. Acta* 50 (2004) 811–816.
- [6] A.K. Ladavos, P.J. Pomonis, *J. Chem. Soc. Faraday Trans.* 87 (1991) 3291–3297.
- [7] R.J.H. Voorhoeve, D.W. Johnson, J.P. Remeika, P.K. Gallagher, *Science* 195 (1977) 827–833.
- [8] J.O.M. Bockris, Z.S. Minevski, *Electrochim. Acta* 39 (1994) 1471–1479.
- [9] J.O.M. Bockris, T. Otagawa, *J. Electrochem. Soc.* 131 (1984) 290–302.
- [10] J.H. White, A.F. Sammells, *J. Electrochem. Soc.* 140 (1993) 2167–2177.
- [11] A. Lan, A.S. Mukasyan, *Ind. Eng. Chem. Res.* 47 (2008) 8989–8994.
- [12] J. Xu, X. Liu, Y. Chen, Y. Zhou, T. Lu, Y. Tang, *J. Mater. Chem.* 22 (2012) 23659–23667.
- [13] R. Dillon, S. Srinivasan, A.S. Arico, V. Antonucci, *J. Power Sources* 127 (2004) 112–126.
- [14] Y. Chen, G. Zhang, J. Ma, Y. Zhou, Y. Tang, T. Lu, *Int. J. Hydrogen Energy* 35 (2010) 10109–10117.
- [15] Y. Chen, Y. Zhou, Y. Tang, T. Lu, *J. Power Sources* 195 (2010) 4129–4134.
- [16] D. Kardash, C. Korzeniewski, N. Markovic, *J. Electroanal. Chem.* 500 (2001) 518–523.

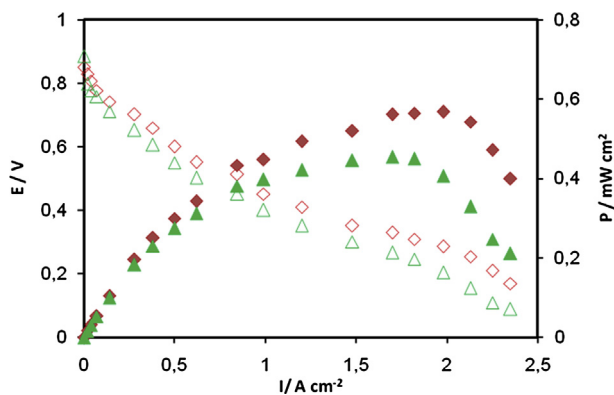


Fig. 10. Cell voltage and power density as a function of current density for the single cell with a commercial 5Pt–15LaFeO₃–2CNT/CC–DL (♦) and 5Pt–15LaFeO₃/CC–DL (▲) catalyst (anode) and Pt–Ru/C catalyst (cathode) operating with humidified CH₃OH/O₂ at 80 °C and 1 atm.

- [17] J.E. Mark, Polym. Eng. Sci. 36 (1996) 2905–2920.
- [18] K. Akamatsu, S. Takei, M. Mizuhata, A. Kajinami, S. Deki, S. Takeoka, M. Fujii, S. Hayashi, K. Yamamoto, Thin Solid Films 359 (2000) 55–60.
- [19] R. Zeng, M.Z. Rong, M.Q. Zhang, H.C. Liang, H.M. Zeng, Appl. Surf. Sci. 187 (2002) 239–247.
- [20] D.H. Cole, K.R. Shull, P. Baldo, L. Rehn, Macromolecules 32 (1999) 771–779.
- [21] P.O. Osifo, A. Masala, J. Power Sources 195 (2010) 4915–4922.
- [22] E. Guibal, Prog. Polym. Sci. 30 (2005) 71–109.
- [23] M.S. Ekrami-Kakhki, M. Khorasani-Motlagh, M. Noroozifar, J. Appl. Electrochem. 41 (2011) 527–534.
- [24] M. Khorasani-Motlagh, M. Noroozifar, M.S. Ekrami-Kakhki, Int. J. Hydrogen Energy 36 (2011) 11554–11563.
- [25] M. Khorasani-Motlagh, M. Noroozifar, A. Ahanin-Jan, J. Iran. Chem. Soc. 9 (2012) 833–839.
- [26] S. Farhadi, Z. Momeni, M. Taherimehr, J. Alloys Compd. 471 (2009) L5–L8.
- [27] B.D. Cullity, R.S. Stock, Elements of X-ray Diffraction, third ed., Prentice-Hall, Inc., 2001.
- [28] H.P. Klug, L.E. Alexander, X-ray Diffraction Procedures, second ed., Wiley, New York, 1964.
- [29] S.M. Khetre, A.U. Chopade, C.J. Khilare, S.R. Bamane, Int. J. Porous Mater. 1 (2011) 1–5.
- [30] A.J. Bard, Electroanalytical Chemistry, Marcel Dekker, New York, 1976.
- [31] D.H. Lim, W.D. Lee, D.H. Choi, H.I. Lee, Appl. Catal. B 94 (2010) 85–96.
- [32] D.N. Prader, J.J. Rusek, Appl. Energy 74 (2003) 135–140.
- [33] H. Yang, L. Dai, D. Xu, J. Fang, S. Zou, Electrochim. Acta 55 (2010) 8000–8004.
- [34] J.H. Kim, S.M. Choi, S.H. Nam, M.H. Seo, S.H. Choi, W.B. Kim, Appl. Catal. B Environ. 82 (2008) 89–102.
- [35] C. Xu, Y. Su, L. Tan, Z. Liu, J. Zhang, S. Chen, S.P. Jiang, Electrochim. Acta 54 (2009) 6322–6326.
- [36] X. Wang, J. Liao, C. Liu, W. Xing, T. Lu, Electrochem. Commun. 11 (2009) 198–201.
- [37] H. Song, X. Qiu, F. Li, Appl. Catal. A 364 (2009) 1–7.
- [38] Y. Ou, X. Cui, X. Zhang, Z. Jiang, J. Power Sources 195 (2010) 1365–1369.
- [39] H. Song, X. Qiu, F. Li, Electrochim. Acta 53 (2008) 3708–3713.
- [40] J. Wang, J. Xi, Y. Bai, Y. Shen, J. Sun, L. Chen, W. Zhu, X. Qiu, J. Power Sources 164 (2007) 555–560.
- [41] T. Huang, J. Liu, R. Li, W. Cai, A. Yu, Electrochem. Commun. 11 (2009) 643–646.
- [42] M. Chen, Z.B. Wang, Y. Ding, G.P. Yin, Electrochem. Commun. 10 (2008) 443–446.
- [43] D.M. Han, Z.P. Guo, R. Zeng, C.J. Kim, Y.Z. Meng, H.K. Liu, Int. J. Hydrogen Energy 34 (2009) 2426–2434.
- [44] T. Huang, D. Zhang, L. Xue, W.B. Cai, A. Yu, J. Power Sources 192 (2009) 285–290.
- [45] D.K. Kang, C.S. Noh, N.H. Kim, S.H. Cho, J.M. Sohn, T.J. Kim, Y.K. Park, J. Ind. Eng. Chem. 16 (2010) 385–389.
- [46] X. Zhong, J. Chen, L. Yang, X. Sun, Indian J. Chem. 47A (2008) 504–509.
- [47] Z. He, J. Chen, D. Liu, H. Zhou, Y. Kuang, Diamond Relat. Mater. 13 (2004) 1764–1770.